FEBRUARY 13 2025

Characterization of fibrous media transport parameters from multi-compression-ratio measurements of normal incidence sound absorption[a)]

Andrea Santoni ; Francesco Pompoli ; Cristina Marescotti; Patrizio Fausti

J. Acoust. Soc. Am. 157, 1185–1201 (2025)
https://doi.org/10.1121/10.0035847

JASA ARTICLE

Characterization of fibrous media transport parameters from multi-compression-ratio measurements of normal incidence sound absorption[a)]

Andrea Santoni,[b)] Francesco Pompoli, Cristina Marescotti, and Patrizio Fausti
Department of Engineering, University of Ferrara, via G. Saragat 1, 44122 Ferrara, Italy

ABSTRACT:
This study presents a novel approach for estimating the transport parameters that characterize the acoustic behavior of fibrous materials using the Johnson-Champoux-Allard equivalent fluid model. We propose an inversion technique, based on an optimization algorithm, to fit the Johnson-Champoux-Allard model's predictions of normal incidence sound absorption coefficient to multi-compression-ratio experimental data. Experimental measurements using the two-microphone technique within an impedance tube are conducted on fibrous material samples tested at various compression ratios. Optimization is performed using both a non-linear programming solver and a genetic algorithm. Validation of the proposed method shows good agreement with well-established techniques and demonstrates its effectiveness across a range of fibrous materials. A sensitivity analysis emphasizes the importance of selecting appropriate boundaries for the search space in the optimization process. To enhance the robustness of optimization, a two-step iterative procedure is proposed. This straightforward methodology offers a robust and reliable framework for characterizing the transport properties of fibrous materials. Its ease of implementation and accuracy make it a valuable tool for enhancing material design and optimization in acoustic engineering.
 https://doi.org/10.1121/10.0035847
(Received 19 September 2024; revised 30 December 2024; accepted 28 January 2025; published online 13 February 2025)
[Editor: Mélanie Nolan] Pages: 1185–1201

I. INTRODUCTION

The equivalent fluid model is a well-established method for analyzing the acoustic behavior of porous and fibrous materials when excited by a sound wave. This model simplifies the description of an acoustic porous material by representing it as an equivalent fluid, characterized by a complex density and dynamic bulk modulus, while assuming a motionless skeleton. Accurate modeling of the acoustic behavior of such materials relies on precise knowledge of physical parameters that link the material's microstructure to its macroscopic response to sound waves. The number and type of physical parameters required depend on the chosen propagation model, which generally falls into one of three categories: (1) empirical models, requiring a limited set of input parameters; (2) micro-structural models, applicable to simplified pore morphologies; and (3) semi-phenomenological models, which treat the porous medium as a compressible and dissipative equivalent fluid defined by several physical parameters.

Although various experimental methods have been developed to directly measure these non-acoustical parameters,[1–5] direct measurement remains challenging, as it requires complex test rigs and procedures.[6,7] Moreover, inter-laboratory studies[8,9] have demonstrated poor reproducibility in experimental parameter estimation, often due to sample preparation inconsistencies and the lack of standardized methods for measuring pore-structure parameters. Currently, only airflow resistivity can be measured using a standardized procedure, as described by ISO 9053.[10,11] In response to these challenges, inverse characterization methods represent a viable alternative for estimating these parameters from standard impedance tube measurements. The literature offers various inverse characterization techniques, ranging from analytical methods that leverage the asymptotic behavior of the equivalent fluid's bulk properties to optimization-based approaches that use algorithms (e.g., non-linear fitting, or genetic algorithms) to identify parameter sets that best approximate the observed acoustic behavior through a chosen wave propagation model.[12–15]

This paper presents a methodological approach for characterizing the transport parameters required to describe the acoustic behavior of fibrous materials using normal incidence sound absorption measurements. The primary objective of this study is to develop and standardize a simple and reliable procedure for characterizing fibrous materials and optimizing their density. This enables the design and optimization of sound absorption panels while significantly reducing the need for extensive prototyping phases. Although several methodologies with the same purpose already exist, to the authors' best knowledge, a similar approach has not been proposed before. In contrast to traditional inverse

[a)]This paper is part of a special issue on Sound Absorption and Diffusion: Modeling, Measurement and Application.
[b)]Email: andrea.santoni@unife.it

characterization methodologies, typically applied to a single material, the proposed methodology links optimization parameters to variations in material density. The main novelty of this approach lies in the idea of constraining optimization-based physical parameters to a density function, representing a substantial shift from conventional inversion techniques, which perform separate minimizations for each material followed by data interpolation. Traditional single-material inversions are notably susceptible to high variability and result dispersion, particularly when applied to the entire set of transport parameters, as discussed by Bonfiglio and Pompoli.[14] As demonstrated by the results presented in this paper, the proposed methodology effectively mitigates these issues.

The proposed inversion technique is developed considering the semi-phenomenological model based on the work of Johnson *et al.*[16] and Champoux and Allard.[17] The Johnson-Champoux-Allard (JCA) equivalent fluid model was chosen because simpler models, such as the monoparametric model developed by Delany and Bazley[18] or the extension proposed by Miki,[19] are not suitable for porosities lower than 90%. Consequently, the JCA multiparametric model was employed, as it can accurately describe also lower porosities associated with high compression rates. It requires five transport parameters to compute the complex density and dynamic bulk modulus of an acoustic dissipative medium: airflow resistivity (σ), porosity (ϕ), tortuosity (α_∞), and the viscous and thermal characteristic lengths (Λ and Λ'). The proposed method provides a straightforward approach for characterizing these five transport parameters as a function of the material's density, using only experimental measurements of the normal incidence sound absorption coefficient, obtained, for example, through the transfer function method described by the ISO 10534-2 standard,[20] on samples of the considered fibrous material at different compression rates. Although the approach is developed and validated using the JCA model, it has the potential to be extended to other models that require different sets of parameters. For instance, it could be adapted to the Johnson-Champoux-Allard-Lafarge equivalent fluid model,[21] which, in addition to the five transport parameters defined for the JCA model, also considers the static thermal permeability (k_0'). This study applies the proposed inverse characterization approach to samples of loose natural fibers and investigates its applicability to other types of fibrous materials. The proposed methodology is limited to fibrous materials, since during compression, the fibers pack closely onto one another, increasing the material's density without deforming their cross-sectional area (i.e., the fibers' radius remains constant). This assumption, however, does not hold for foam-like porous materials, where compression may cause deformation of the porous cells in addition to increasing the material's density.

The proposed approach is described in detail in Sec. II. The different materials considered in this study are detailed in Sec. III. In Sec. IV, the accuracy of the proposed method is evaluated by comparing the normal incidence sound absorption predicted by the JCA model with experimental results. Additionally, the reliability of the estimated transport parameters is validated by comparing them with values obtained from well-established methods.

II. INVERSE CHARACTERIZATION

A. Acoustical model for sound absorption

The acoustic behavior of porous and fibrous media with stiffness or density greater than the fluid filling the pores can be analyzed through an equivalent fluid model: a homogenization approach to describe sound wave propagation in a porous medium, considered as an equivalent dissipative fluid. In the equivalent fluid model, the material is characterized by a complex density $\widetilde{\rho}_c$ and a dynamic bulk modulus $\widetilde{K}_c$, assuming a motionless skeleton.[22,23] This model takes into account thermal and viscous effects due to the interaction of sound waves and the medium's microstructure. These effects can be computed separately, assuming that the wavelength is much larger than the average pore size. The JCA model describes visco-inertial dissipative effects inside the porous media using five physical parameters: ϕ, σ, α_∞, Λ, and Λ', respectively, the open porosity, the static airflow resistivity, the high frequency limit for the tortuosity, and the viscous and thermal characteristic lengths. In the JCA framework, the frequency-dependent complex density $\widetilde{\rho}_c$, associated with the inertial and viscous forces, is expressed as follows:

$$\widetilde{\rho}_c = \frac{\alpha_\infty \rho_0}{\phi}\left[1 + \frac{\sigma\phi}{\mathrm{j}\omega\alpha_\infty\rho_0}\sqrt{1 + \mathrm{j}\frac{4\eta\alpha_\infty^2\rho_0\omega}{\sigma^2\Lambda^2\phi^2}}\right], \tag{1}$$

while the complex frequency-dependent dynamic bulk modulus $\widetilde{K}_c$, taking into account the thermal exchanges between the frame and fluid, is determined as follows:

$$\widetilde{K}_c = \frac{\gamma P_0/\phi}{\gamma - (\gamma-1)\left[1 - \mathrm{j}\frac{8\eta}{\rho_0\omega P_r\Lambda'^2}\sqrt{1 + \frac{\mathrm{j}\rho_0\omega P_r\Lambda'^2}{16\eta}}\right]^{-1}}, \tag{2}$$

where ρ_0 is the density of air, ω is the angular frequency, γ is the heat capacity ratio, P_r is the Prandtl number, η is the dynamic viscosity of air, and P_0 is the ambient pressure.

The characteristic impedance Z_c of the equivalent fluid medium and the complex wavenumber k_c can be computed from the complex density and bulk modulus given in Eqs. (1) and (2), as follows:

$$Z_c = \sqrt{\rho K}, \tag{3}$$

$$k_c = \omega\sqrt{\frac{\rho}{K}}. \tag{4}$$

Considering a porous material of thickness h placed on a rigid reflecting boundary, the surface impedance for normal incidence Z_s is given by the following:

https://doi.org/10.1121/10.0035847

$$Z_s = -\mathrm{j}Z_c\cot(k_c h), \tag{5}$$

the normal incidence sound absorption coefficient α_n is finally evaluated as follows:

$$\alpha_n = \frac{4\mathrm{Re}\left\{\frac{Z_s}{\rho_0 c_0}\right\}}{\left|\frac{Z_s}{\rho_0 c_0}\right|^2 + 2\mathrm{Re}\left\{\frac{Z_s}{\rho_0 c_0}\right\} + 1}, \tag{6}$$

where c_0 represents the speed of sound in air. The normal incidence sound absorption, computed using Eq. (6) based on the JCA model, is used to define the cost function employed by the minimization algorithm to estimate the transport parameters of the model, as described in Sec. II B.

B. Transport parameters

Eqs. (1) and (2) depend on five transport parameters, which represent the solution sought from the minimization-based inversion algorithm and are described by analytical or empirical equations. The key assumption of this approach is that the transport parameters depend on the material's density, which increases proportionally with the compression rate applied to the fibers.

The open porosity ϕ, measuring the fractional amount of air volume in the interconnected pores of the considered material. It can be evaluated as the ratio between the air volume V_f and the total volume V_t of the investigated material (which is the sum of fluid volume and volume of the skeleton V_s). It can be proven that the porosity can be alternatively computed from the ratio between the bulk density of the porous material ρ and density of the solid skeleton ρ_s,

$$\phi = \frac{V_f}{V_{tot}} = 1 - \frac{\rho}{\rho_s}. \tag{7}$$

The static airflow resistivity σ, defined as the ratio between the static pressure gradient and the fluid velocity across the material, is computed through an analytical equation proposed Tamayol *et al.*[24] for 2D cylinders having equal radii and square location according to model as follows:

$$\sigma = \frac{\eta}{(2r_e)^2} \frac{\sqrt{1-(1-\phi)}}{C_1\left(\frac{C_2}{1-\phi} - 3\sqrt{\frac{c_2}{1-\phi}} + 3 - \sqrt{\frac{1-\phi}{C_2}}\right)}. \tag{8}$$

As expressed by Eq. (8), the airflow resistivity only depends on the material's porosity and the fibers' radius. The coefficient $C_1 = 0.21$ and $C_2 = 0.71$ were used, as proposed by Pompoli and Bonfiglio[25] extending the model considering a randomly assembled radii distributions. Fibrous materials, whether natural or synthetic, typically exhibit a range of fiber diameters, known as polydisperse diameter distribution. The term r_e in Eq. (8) physically represents the effective radius of the equivalent homogeneous monodisperse fiber material, as already been used in previous works.[26] The effective radius r_e is one of the design parameters of the multi-variable function to be optimized. While this simplified model assumes that the fibers are oriented parallel to the flow direction, fibrous materials typically exhibit either 2D or 3D orientations. Studies have shown that fiber orientation significantly influences transport parameters, particularly airflow resistivity.[27,28] Additionally, fibers orientation is affected by the degree of compression. Castagnede *et al.*[29] proposed a model for evaluating airflow resistivity that accounts for material compression, which was later refined by Hirosawa and Nakagawa.[30] Lei *et al.*[31] further explored the impact of 3D fiber arrangements on airflow resistivity, incorporating geometric considerations to calculate fiber rotation as a function of compression. However, the proposed approach neglects fibers orientation, as incorporating it would require a 3D analysis of the initial fibers distribution. Instead, we aim to develop an easily implementable model that requires only experimental data commonly measured in most acoustic laboratories.

The high-frequency limit of tortuosity α_∞, a dimensionless parameter related to the complexity of the pathways of a sound ways propagating through the medium pores, is computed using Archie's empirical law[32] based on the material's porosity as follows:

$$\alpha_\infty = \left(\frac{1}{\phi}\right)^{\beta}. \tag{9}$$

The constant β depends on the microstructure of the porous medium. Different values of β can be found in the literature, derived under specific assumptions.[33] While it could be considered as an additional variable to be determined in the inversion process, the fixed value $\beta = 0.9574$ is considered, as computed in Ref. 25 independently from the fiber's radius.

The viscous Λ characteristic length is a geometrical quantity related to the scale of the pores concerned with viscous losses. The viscous characteristic length is determined from the material's porosity using the empirical formulation proposed by Pompoli:[34]

$$\Lambda = A_1 r_e (1-\phi)^{-A_2}. \tag{10}$$

Analogously, the thermal characteristic length Λ', related to the scale of the pores associated with thermal losses, is determined as follows:

$$\Lambda' = A_3 r_e (1-\phi)^{-A_4}. \tag{11}$$

The design variables A_1, A_2, A_3, and A_4 represent unknown constants dependent on the material, to be determined through the minimization-based inversion procedure, together with the effective radius r_e, by plugging Eqs. (7)–(11) into the expressions to determine the equivalent

fluid complex density and dynamic bulk modulus, given in Eqs. (1) and (2).

C. Optimization algorithm

The proposed approach employs an optimization algorithm to estimate the coefficients r_e and A_i required by Eqs. (8)–(11) introduced in Sec. II B, to determine three of the five transport parameters used as input data by the JCA model (σ, Λ, and Λ'). The optimization aims to determine a set of design variables, $x = \{x_1, x_2, \ldots, x_n\}$, by minimizing an objective function $\mathcal{F}(x)$. The objective function of the considered optimization problem is defined in terms of the normalized sound absorption coefficient difference as follows:

$$\mathcal{F}(x) = \sum_{i=1}^{n} \frac{1}{n} \sum_{l=1}^{m} \frac{1}{m} \left| \alpha_{n,JCA,i,l} - \alpha_{n,\exp,i,l} \right|, \tag{12}$$

where $\alpha_{n,\exp,i,l}$ represents the value of the normal incidence absorption coefficient measured according to ISO 10534-2,[20] on material samples tested at different densities ρ, by varying the compression ratio of the loose fibers. The compression ratio is typically defined as the ratio of the sample density to its initial density and is further discussed in the following section. While $\alpha_{n,JCA,i,l}$ is the value predicted using Eq. (6) based on the JCA model. Both quantities are evaluated at the lth frequency and the ith compression ratio. As expressed in Eq. (12), the optimization is implemented to minimize the global error between the experimental and predicted data, summed over m frequency lines and n investigated densities or compression ratios. The minimization of the objective function is subject to a set of inequality constraints $\mathcal{G}(x) \leq 0$ to ensure consistency between the numerical values representing a mathematically optimal solution and the physical meaning of transport parameters. Moreover, lower and upper bounds for each design variable are defined to limit the solution space over which the optimal set of values is sought: $x_{\text{lb}} \leq x \leq x_{\text{ub}}$. The characteristics of the objective function, the number of design parameters, the number of constraints, and the boundaries of the problem significantly affect the efficiency of the algorithm and the accuracy of the solutions. Additionally, different solvers can be employed in the algorithm.

All these relevant aspects concerning the code implemented for the proposed approach are illustrated and discussed in this paragraph. The implemented algorithm considers five design parameters, each with specific boundaries as follows:

$$[x_{\text{lb}}, x_{\text{ub}}] : \begin{cases} x_1 = r_e \cdot 10^{-6}, & x_{lb,1} \leq x_1 \leq x_{ub,1}, \\ x_2 = A_1, & x_{lb,2} \leq x_2 \leq x_{ub,2}, \\ x_3 = A_2, & x_{lb,3} \leq x_3 \leq x_{ub,3}, \\ x_4 = A_3, & x_{lb,4} \leq x_4 \leq x_{ub,4}, \\ x_5 = A_4, & x_{lb,5} \leq x_5 \leq x_{ub,5}. \end{cases} \tag{13}$$

While design variables x_2 to x_5 are non-dimensional coefficients, x_1 represents the effective radius of the fibers, expressed in μm to avoid scaling issues, typically associated with multi-parametric optimization when search spaces involve design parameters of different scales. The main challenges associated with optimization algorithms involving design parameters of significantly different scales are related to defining an adequate step size and a meaningful stopping criterion. These issues can be mitigated by appropriately scaling optimization parameters to vary within comparable ranges of magnitude. Both solvers employed require the definition of the search space limits. Ideally, specific lower and upper boundary values would be defined for each investigated material, reflecting its unique characteristics. However, the rationale behind this methodology is its applicability to characterizing fibrous materials without prior knowledge of their microstructure. Therefore, general boundaries that broadly cover the range of values of interest for fibrous materials with potential acoustic applications can be defined. Based on the literature, values provided in Table I are used as the lower and upper boundaries, $x_{lb,i}$ and $x_{ub,i}$, with $i = 1, 2, \ldots, 5$, for all the investigated materials presented in Sec. III.

Additional behavioral conditions are imposed on the optimization algorithm through inequality constraints, both to limit the value of transport parameters, which depend on the design variables x_1, within a specified range, and to express possible relationships between the physical parameters that must be fulfilled. The following conditions expressing relationships between the transport parameters, or limiting values within a realistic range of values for acoustic fibrous materials, constitute the inequality constraints of the optimization problem as follows:

$$\mathcal{G}(x) : \begin{cases} \Lambda \leq \Lambda', \\ 1\ \mu\text{m} \leq \Lambda \leq 1000\ \mu\text{m}, \\ \Lambda' \leq 2000\ \mu\text{m}, \\ 10^2\ \text{Ns/m}^4 \leq \sigma \leq 10^5\ \text{Ns/m}^4. \end{cases} \tag{14}$$

It is worth mentioning that no constraints are imposed on the value of the tortuosity α_∞, as this parameter is not obtained from the inversion algorithm but computed as a function of the material's porosity ϕ through Eq. (9). A flow chart diagram to illustrating the proposed approach is presented in Fig. 1.

Different solvers can be employed to compute the optimal solution minimizing the objective function $\mathcal{F}(x)$ while fulfilling the constraints $\mathcal{G}(x)$. Two different approaches are

TABLE I. Lower and upper boundaries imposed for each design parameter in the minimization process.

	x_1	x_2	x_3	x_4	x_5
x_{lb}	0.1 μm	0.001	0.100	0.001	0.100
x_{ub}	50.0 μm	4.000	2.000	6.000	2.000

https://doi.org/10.1121/10.0035847

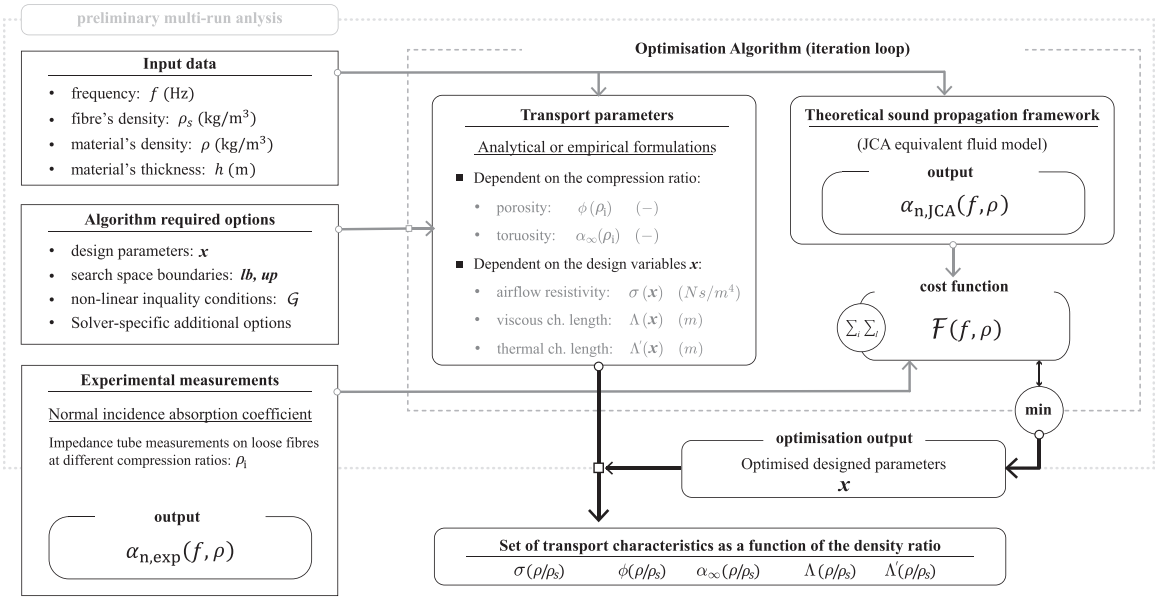

FIG. 1. Schematic illustration of proposed inversion approach proposed to characterize the transport parameters of fibrous material.

tested for the minimization code implemented in MATLAB (for more detailed and practical information concerning the employed solvers, refer to the documentation of the Optimization Toolbox):

- `fm`: a non-linear programming solver used to find the minimum of constrained non-linear multi-variable functions. It requires the definition of the objective function, an initial guess of the design variables $\{\mathbf{x}_0\}$, possible boundaries, and linear or non-linear constraints. This class of solvers is implemented in MATLAB through the function `fmincon`, which offers differs algorithms. In the proposed approach, optimization is performed using the `internal-point` algorithm.[35,36]
- `ga`: a genetic algorithm solver. The minimum of constrained or unconstrained functions is obtained through a search-based approach, operating on the basic principles of genetics and natural selection. At each iteration step, this algorithm randomly selects individuals from the current population as parents to breed children for the next generation.[37] Generation after generation, the population evolves toward the optimal solution. This class of solvers is implemented in MATLAB through the function `ga`, which offers requires the definition of the objective function, the population size, possible boundaries, and linear or non-linear constraints.

These functions thus provide two optimization algorithms that search the solution space in different ways:[38] `fmincon` is a gradient-based optimization algorithm highly effective when the problem is smooth and differentiable, while `ga` is a derivative-free optimization technique that does not require the objective function to be smooth or differentiable, nor the *a priori* definition of starting values. The need in the solver `fmincon` for initial guess values to be specified is relevant, as it can significantly affect the accuracy and reliability of the results. A poor initial guess may lead to convergence to a suboptimal solution, especially in problems with multiple local minima. Strategies to reduce such risk have been developed, such as using a multi-start approach or hybrid solutions combining non-linear programming and genetic algorithms. Further considerations on this aspect are provided in Sec. IV, where the results obtained through the two different solvers are compared and discussed.

The accuracy and efficiency of solvers implemented in MATLAB, as in any other commercial or open-source software for numerical computing, can be enhanced by appropriately setting optimization tolerances, which define stopping criteria and convergence. For the problem at hand, this is a non-trivial task. Although the employed solvers have predefined default values, it is worthwhile to analyze how the results might be influenced by non-optimal settings. To this end, three different optimization tolerances for the non-linear programming solver are considered:

- `Optimality tolerance`: This tolerance is associated with the first-order optimality measure. The solver stops when the optimality measure becomes smaller than this tolerance.
- `Step tolerance`: This tolerance represents the lower bound for the step size. The solver stops when the step size required by optimization becomes smaller than this tolerance.
- `Max iterations`: These iterations specify the maximum number of iterations allowed for optimization. The solver stops once this value is reached.

Figure 2 shows the evolution of the cost function $\mathcal{F}(x)$ across iterations for each tolerance. In each case, the tolerance under investigation is varied independently, while the other two are set to values that do not influence the stopping

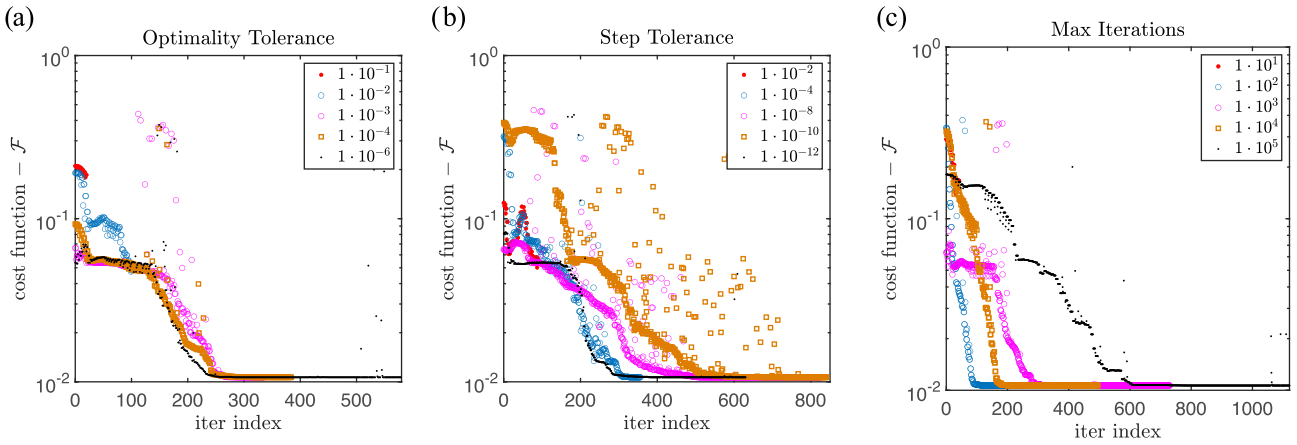

FIG. 2. Influence of different optimization tolerances on the convergence of the cost function $\mathcal{F}(x)$: (a) optimality tolerance; (b) step tolerance; and (c) maximum iterations.

criteria. Figure 2(a) illustrates the effect of varying the optimality tolerance. Convergence is achieved when the tolerance value is set to 10^{-3}. For smaller optimality tolerances, the cost function converges to the same value, but the computational time required increases significantly. Conversely, for larger tolerances, the optimization algorithm fails to converge. Figure 2(b) shows the impact of the step tolerance. The optimization algorithm begins to converge when this tolerance is set to 10^{-4}. Larger tolerance values result in inaccurate solutions, as the stopping criteria prevent the cost function from being adequately minimized. While further reductions in the step tolerance still allow convergence, they also increase the computational cost without improving accuracy. Figure 2(c) demonstrates the influence of the maximum number of iterations. Convergence is only achieved when this parameter is set to 10^2 or higher.

III. MATERIALS AND EXPERIMENTAL METHOD

Experimental tests are carried out at the Engineering Department of the University of Ferrara to measure the normal incidence sound absorption of various fibrous materials. A total of ten types of fibers are considered in this study to investigate the applicability of the method to a wide range of acoustic fibrous materials, including both petroleum-based and natural fibers. These materials include polyester fibers (PF), cotton fibers (CF), glass fibers (GF), jute fibers (JF), various types of hemp fibers (HF_t), differing especially in the treatment t they underwent through, and *Posidonia oceanica* fibers (AF), All the investigated fibers, their characteristics, and the range of investigated bulk densities $[\rho_{min}, \rho_{max}]$ are summarized in Table II.

Loose fibers of each material are tested in an impedance tube with a diameter of 45 mm at different compression ratios. As previously mentioned, the compression ratio is typically defined as the ratio of the sample density to an initial density. For loose fibers, the initial density only represents an arbitrary reference value. Nevertheless, the concept of compression ratio remains useful for identifying a set of samples that are progressively compressed to a smaller thickness h, resulting in a higher density ρ and, according to Eq. (7), a lower porosity ϕ. The experimental procedure involves measuring the normal incidence sound absorption on samples of loose fibers. A precise amount of fibers is weighed and manually compacted into a cylindrical sample to fit the sample holder of the 45-mm impedance tube. The sample holder is mounted on the impedance tube, backed by a rigid reflective plate. Thanks to an acoustically transparent mesh mounted within the tube to constrain the loose fibers, the compression ratio (i.e., the material density) can be incrementally increased by sliding the backing plate, allowing for precise control over the desired thickness. The sound absorption coefficient is measured each time the fibers within the sample holder are progressively compressed to the thicknesses associated with all the densities within the range of investigation. The entire test procedure is illustrated in Fig. 3.

The proposed inversion approach is designed to estimate the transport parameters of fibrous materials as a function of its density, based on the experimental normal incidence sound absorption. Therefore, it can be applied to

TABLE II. Investigated fibrous materials.

ID	$\rho_{\min}$ kg/m^3	$\rho_{\max}$ kg/m^3	ρ_s kg/m^3	Material type
AF	48	180	1518	*Posidonia oceanica* fiber (Ref. 34)
JF	75	145	1300	Jute fiber
HF_{car}	59	176	1300	Hemp fiber, carding (CAR in Ref. 26)
HF_{NaOH}	59	176	1300	Hemp fiber, alkaline (NaOH in Ref. 26)
HF_{WTC}	59	176	1300	Hemp fiber, combing (WTC in Ref. 26)
HF_{FTC}	59	176	1300	Hemp fiber, combing (FTC in Ref. 26)
HF_{cot}	81	217	1300	Hemp fiber, cotonization process
CF	51	193	1500	Cotton felt fiber (F in Ref. 39)
PF	48	181	1370	Polyester fiber (H in Ref. 39)
GF	39	142	2000	Glass fiber (glass wool)

https://doi.org/10.1121/10.0035847

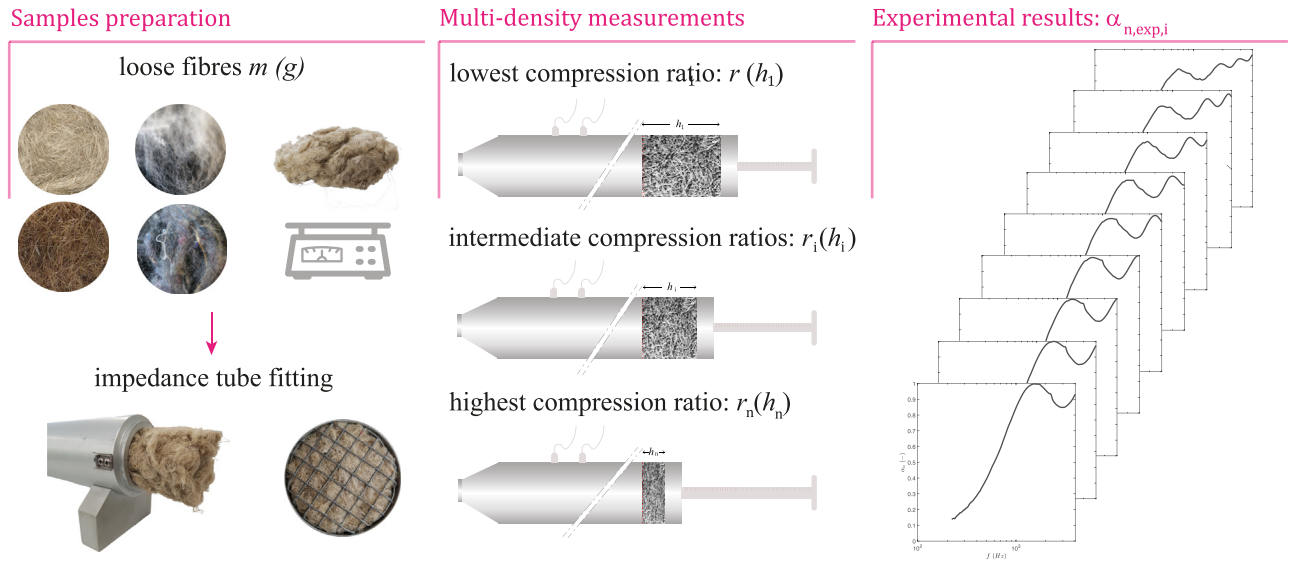

FIG. 3. Schematic illustration of the experimental procedure to obtain the results used by the optimization algorithm.

measurements using the transfer function approach, according to the standard ISO 10534-2,[20] or other experimental techniques, such as the three-microphone transfer matrix method.

IV. RESULTS AND VALIDATION

The main results of the proposed approach and their validation are presented in this section. The following paragraph analyzes and discusses the accuracy of the optimized transport parameters. The transport parameters obtained from the proposed approach as functions of the material porosity [i.e., density functions according to Eq. (7)] are compared with target values derived from a well-established inversion technique based on the measurement of a single sample, described in Ref. 14, and referred to as the "hybrid method." Section IV B compares the experimental normal incidence sound absorption coefficient with the predictions of the JCA model obtained from optimization output. The set of design parameters used to compute the results shown in these first two subsections (and in the Appendix) is finally presented in Sec. IV C, which examines the influence of the initial guesses on the accuracy of optimization output and introduces an iterative process to enhance the robustness of the proposed approach.

A. Transport parameters

This section validates the proposed methodology by comparing the transport parameters obtained through our optimization approach, either using the `fm` and `ga` solvers, with the values derived from well-established methods. The validation focuses on Posidonia fibers, selected due to the extensive dataset available for this material. Figure 4 compares the transport parameters for Posidonia fibers (AF) as a function of porosity, using values obtained from our method and those from different consolidated approaches.

Figure 4(a) compares the airflow resistivity curve, $\sigma_{min()}$, evaluated as a function of porosity ϕ using Eq. (8) and the effective radius r_e obtained from the optimization approach, with airflow resistivity values, σ_a, determined from the experimental dynamic density ρ_c using the relationship proposed by Panneton and Olny,[12] which defines σ_a as the low-frequency limit of the imaginary part of the dynamic density as follows:

$$\sigma_a = \lim_{\omega \to 0} (\mathrm{Im}\{\widetilde{\rho}_c\}\omega). \tag{15}$$

For this purpose, the complex density of the fibrous material samples was determined experimentally through impedance tube measurements using the three-microphone technique.[40] While the proposed characterization methodology can be implemented using traditional sound absorption measurements in accordance with the standard ISO 9053,[10,11] the three-microphone technique also enabled the experimental evaluation of airflow resistivity on the same samples tested for the normal incidence sound absorption coefficient. Experimentally evaluating both the optimization input data and the airflow resistivity values, used for validation, under identical conditions avoids the introduction of additional experimental uncertainties. Such uncertainties, which may arise from variations in fiber distribution or boundary conditions, can be particularly significant when working with samples derived from loose fibers.

The minimized curves, labeled as $_{fm}$ and $_{ga}$, show negligible differences between the outputs of the optimization solvers, indicating good consistency. The two curves almost overlap across the entire range of investigated porosities, closely approximating the trend of the airflow resistivity values estimated from Eq. (15). It is worth addressing the deviations observed between the optimized density curve $\sigma_{\mathrm{min}()}$ and the individual values of airflow resistivity σ_a, which increase at higher porosities. It should be noted that Eq. (8), which relates airflow resistivity to the equivalent radius r_e, is derived under the simplifying assumption of a

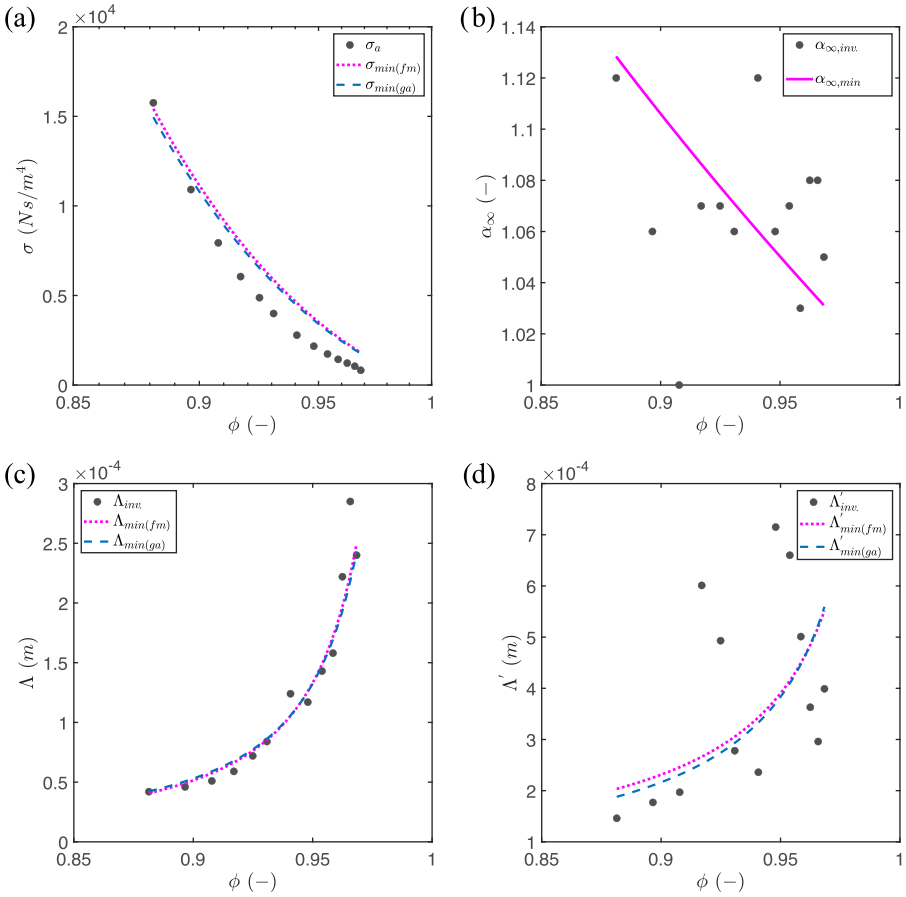

FIG. 4. Comparison of transport parameters for fibers AF obtained from the proposed method and established approaches, plotted against porosity: (a) airflow resistivity; (b) tortuosity; (c) viscous characteristic length; and (d) thermal characteristic length.

two-dimensional unidirectional orientation of the fibers, perpendicularly aligned to the airflow. However, in experimental configurations employing samples of loose fibers, the fibers are generally characterized by a random three-dimensional distribution and orientation, particularly at lower compression ratios, which correspond to higher porosity values. As the compression increases, the fibers tend to gradually align closer to the conditions assumed by Eq. (8). For this reason, in Fig. 4(a), better agreement between the optimized curves $\sigma_{\min()}$ and the target values σ_a occurs at lower porosities, while slight deviations arise as the porosity increases. As the porosity increases, slight deviations arise, as the assumptions underlying Eq. (8) are not fully satisfied under experimental conditions.

The remaining transport parameters used to describe the investigated materials as equivalent fluids through the JCA model, derived from the proposed characterization approach, are compared to values obtained using a well-established minimization-based inversion technique described in Ref. 14. Similar to the proposed methodology, this approach minimizes the difference between the experimental normal incidence sound absorption and the curve estimated through the JCA model, although in this case, it is applied to each individual measurement.

Tortuosity is directly evaluated as a function of the porosity from Eq. (9), rather than being obtained through the optimization algorithm. Figure 4(b) compares the curve adopted in the proposed approach ($\alpha_{\infty,\min}$) with values resulting from the inversion performed at each compression ratio ($\alpha_{\infty,\text{inv.}}$). While the inverted values exhibit significant scatter, making it difficult to discern a clear trend, the curve representing tortuosity computed using the proposed approach lies within the range of scatter across the entire porosity range. This demonstrates the suitability of Eq. (9) for estimating tortuosity as a function of porosity.

Figures 4(c) and 4(d) compare the minimized viscous and thermal characteristic lengths [$\Lambda_{\min()}$ and $\Lambda'_{\min()}$, respectively] with values ($\Lambda_{\text{inv.}}$ and $\Lambda'_{\text{inv.}}$) derived from the same inversion approach, already introduced discussing the tortuosity. Figure 4(c) shows that the density-function curves $\Lambda_{\min()}$, obtained through the optimization algorithm using either one of the implemented solvers, are in perfect agreement with the values of the viscous characteristic length $\Lambda_{\text{inv.}}$ obtained for each investigated compression ratio through the traditional inversion approach. On the other hand, as shown in Fig. 4(d), the inversion approach provides sparse values of the thermal characteristic length $\Lambda'_{\text{inv.}}$, making it difficult to identify a consistent trend. Nevertheless, the minimized curve $\Lambda'_{\min()}$ remains within the range of the target values across the entire porosity range. Minimal differences are observed between the curves obtained from the two solvers for both characteristic lengths.

B. Sound absorption

To further analyze the accuracy and reliability of the proposed approach, a comparison is made between the experimental normal incidence sound absorption coefficients and the results simulated using the JCA model. The

https://doi.org/10.1121/10.0035847

transport parameters used as input data for the JCA model are determined from the design parameters estimated through the proposed inversion technique. Figure 5 compares the experimental normal incidence sound absorption coefficients of Posidonia fibers (AF) against the simulated results from the JCA model, for varying porosities, ranging from $\phi = 0.968$ to 0.881 $\phi = 0.968$ to 0.881. The comparison reveals a remarkable agreement between the simulated results obtained using both the `fm` and `ga` algorithms. For all investigated porosities, the spectra overlap closely. Moreover, the simulation accurately approximates the experimental sound absorption coefficient spectra for all the different porosities within the investigated range. While minor deviations are observed at both lower and higher porosities, the simulations exhibit an overall good accuracy.

To further validate the method across a broader range of fibrous materials commonly used in acoustic mitigation systems, the proposed inversion technique was applied to various types of fibers. The accuracy of the methodology is assessed by comparing the experimental normal incidence sound absorption coefficients with the JCA model simulations, using the estimated transport parameters across

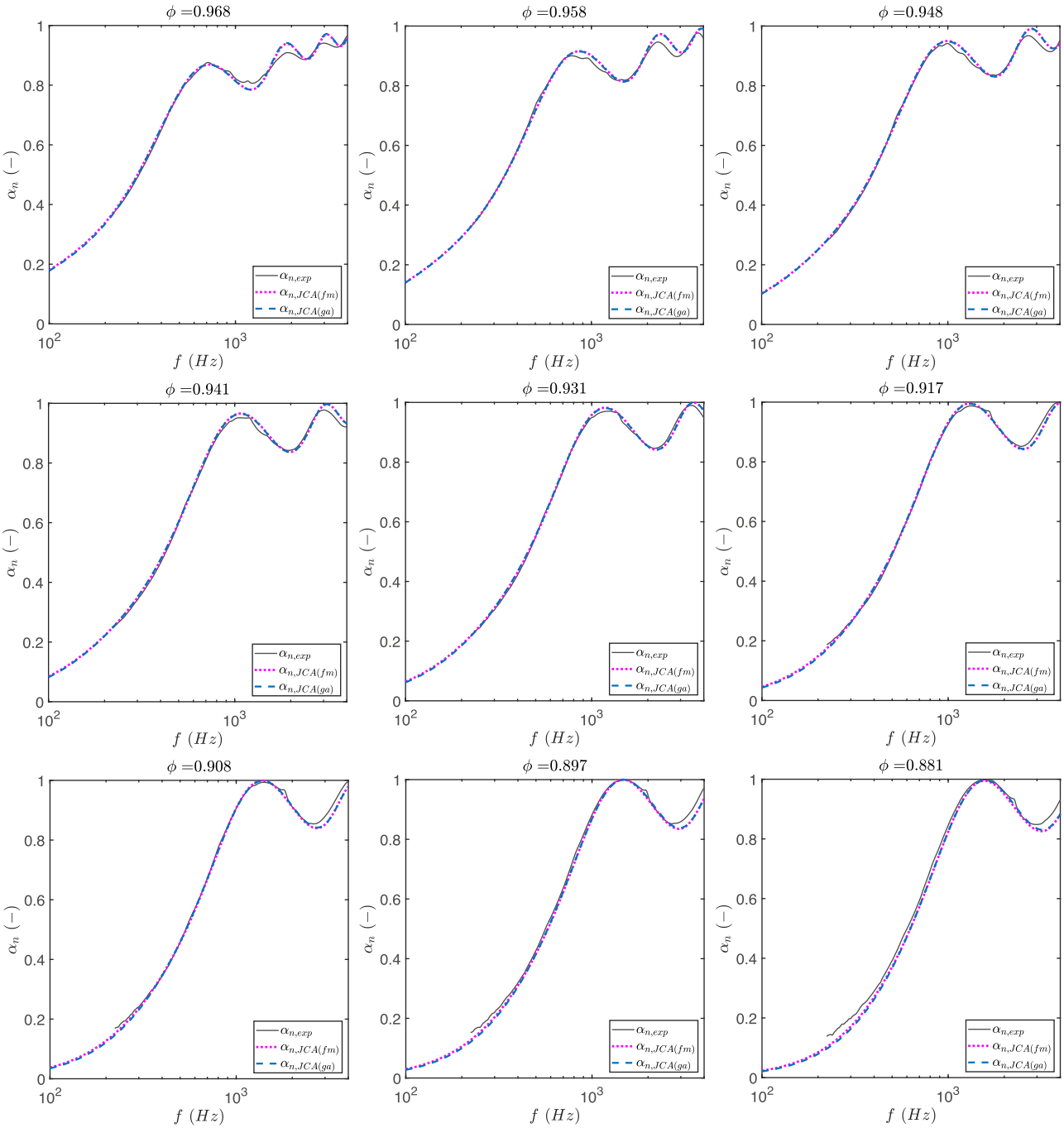

FIG. 5. Fibers AF. Comparison for different values of porosity ϕ between the experimental normal incidence sound absorption coefficient $\alpha_{n,\mathrm{exp}}$ and the JCA model simulations using the inverted transport parameters obtained either from `fm` and `ga` algorithms: $\alpha_{nJCA,fm}$, $\alpha_{nJCA,ga}$.

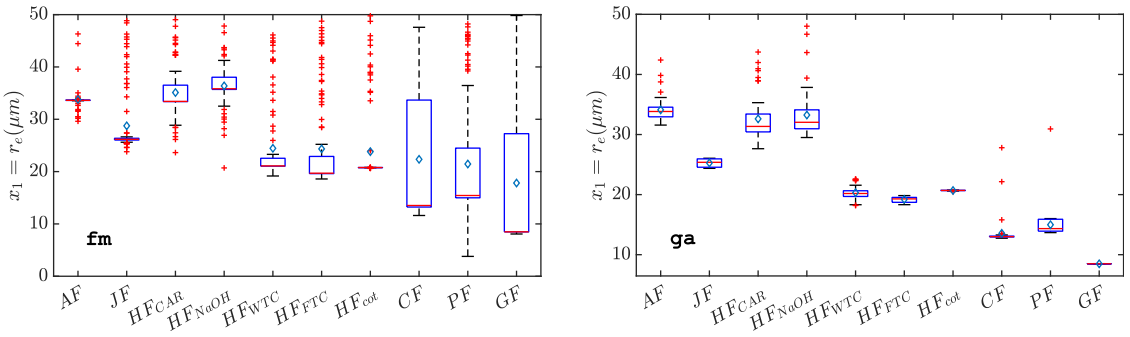

FIG. 6. Statistical distribution associated with the design parameter $x_1 = r_e$ obtained with the `fm` and `ga` solvers.

different porosities. The same observations and conclusions drawn from Fig. 5 apply to the results for each investigated material, presented in the Appendix to enhance readability of this manuscript.

A notable consistency is observed between the results obtained from the two solvers used in the optimization algorithm, both in terms of transport parameters and sound absorption coefficients. However, achieving this consistency requires careful management to avoid convergence to local minima, as discussed in the following paragraph.

C. Influence of the search space

As demonstrated in the previous paragraphs, the design parameters obtained through the optimization process provided reliable predictions of the transport parameters; and consequently, accurate estimations of the normal incidence sound absorption coefficient. Furthermore, strong consistency is observed between the two optimization solvers. However, it must be emphasized that all optimization algorithms are influenced by the choice of initial guess values. The accuracy and consistency observed in the presented results can only be achieved by minimizing the risk of the optimization solver converging to local minima, which may result in mathematically acceptable but physically meaningless outcomes. To investigate how the initial guess may affect optimization output, a parametric analysis is performed by executing multiple runs of the algorithm while randomly varying the set of initial guess values. For the non-linear solver, initial guess values were randomly selected within the search space defined in Table I. Similarly, multiple runs of the genetic algorithm (ga) inherently randomized the starting populations.

The box plots in Fig. 6 represent the statistical distributions of the effective radii ($x_1 = r_e$ in μm) obtained from 100 runs of the optimization algorithm using the `fm` and `ga` solvers. The results indicate a greater spread in outcomes with the non-linear solver (`fm`) compared to the genetic algorithm (ga). For most materials, the non-linear solver exhibits a larger interquartile range (IQR), representing 50% of the data between the first ($Q_1 = 25\%$) and third quartiles ($Q_3 = 75\%$).

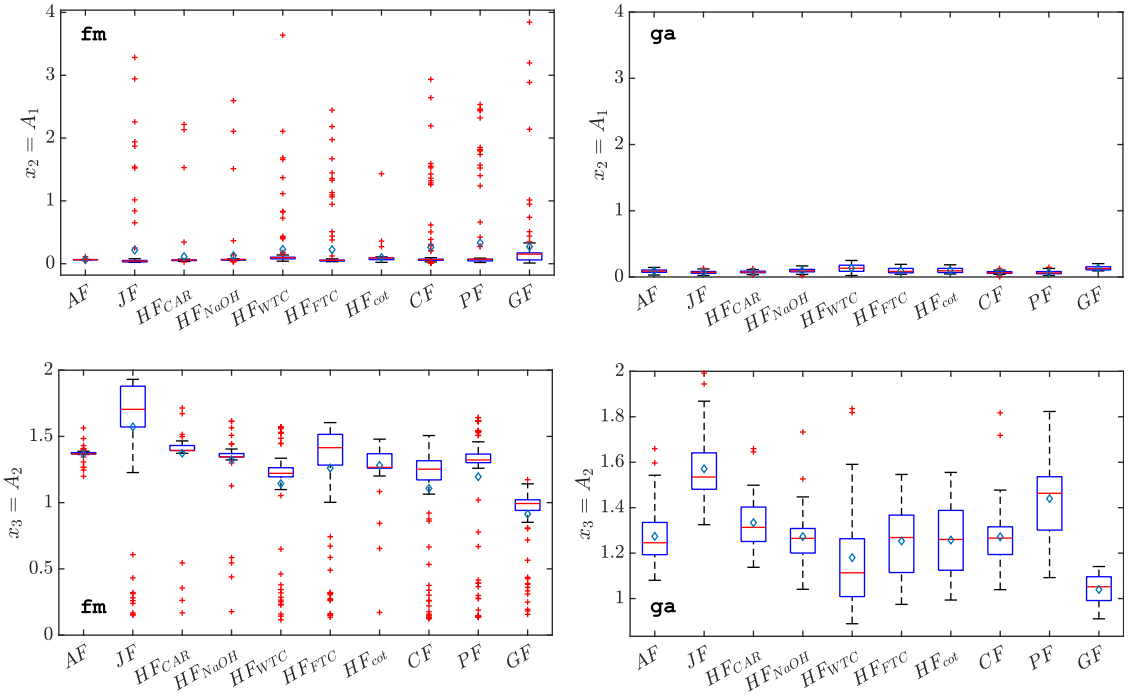

FIG. 7. Statistical distribution associated with the design parameters $x_2 = A_1$ and $x_3 = A_2$ obtained with the `fm` and `ga` solvers.

https://doi.org/10.1121/10.0035847

For materials such as CF, PF, and GF, where the largest IQR is observed, a correspondingly large standard deviation is also noted when `fm` is employed, as indicated by the dashed boxplot whiskers. The red line inside each box represents the median, while blue diamond markers represent the mean, which is reported for completeness even though the former is a better descriptor of the central tendency of the data. The substantial number of outliers, indicated as red crosses, suggests that the `fm` solver is potentially more prone to converging to local minima compared to the ga solver, for which the presence of outliers is limited.

Similarly, the statistical distributions of the design variables x_2 and x_3, associated with the evaluation of the viscous characteristic length Λ, and x_4 and x_5, associated with the thermal characteristic length Λ', are shown in Figs. 7 and 8, respectively. Both solvers yield minimal spread in the results for x_2, with ga consistently producing tightly clustered outcomes, while `fm` shows a larger number of outliers. Conversely, x_3 exhibits a wider spread with both solvers, other the presence of outliers, which is still more emphasized when `fm` is used. This trend is consistently observed across all materials investigated. Parameters x_4 and x_5 generally exhibit greater deviations, regardless of the solver used. This indicates that the thermal characteristic length Λ' has a smaller influence on the sound absorption coefficient results produced by the JCA model, allowing multiple values to yield mathematically equivalent solutions. The variation in results, reflected in a higher standard deviation, is not uniform across materials, and no clear trend is identifiable. The primary difference between the solvers remains the higher number of outliers associated with `fm`.

Overall, the parameters for all materials exhibit either consistent convergence with minimal spread or a larger variation spread over a broader range of values. However, the results do not cluster at the boundaries of the search space, indicating that the imposed limits do not unduly constrain the algorithm or force its convergence. The genetic algorithm (ga) consistently yields more reliable results, with fewer outliers. Nevertheless, neither solver completely eliminates the risk of local minima. This risk can be mitigated by imposing stricter boundaries, by determining the upper and lower boundaries x_{lb} and x_{ub} from the IQRs identified from Figs. 6–8, thus limiting the search space within the first and third quartiles of the parametric optimization results.

A two-step approach is proposed, introducing a second iteration of the optimization process within the IQR-narrowed search space. This significantly reduces both the spread of results and the presence of outliers, yielding very consistent design variables with minimal spread, as shown by the design parameters and associated standard deviation given in Table III. The values represent the coefficient from which transport parameters; and consequently, the absorption coefficient, are computed as a function of material compression ratio, as presented in previous paragraphs. The almost negligible standard deviation associated with optimization output obtained on an IQR-narrowed search space, indicates a minimal spread of the results obtained by multiple runs of optimization. Furthermore, a higher degree of consistency is observed between the two solvers. The difference in the effective radius estimate r_e is generally less than 1 μm, except for H_{CAR} and H_{NaOH}, where differences of 1.7 and 2.8 μm, respectively, are observed. However, larger deviations are found between the solvers for the material-dependent variables A_1, A_2, A_3, and A_4, used to compute the viscous and thermal characteristic lengths according to Eqs. (10) and (11). Differences for A_1 range between 10%

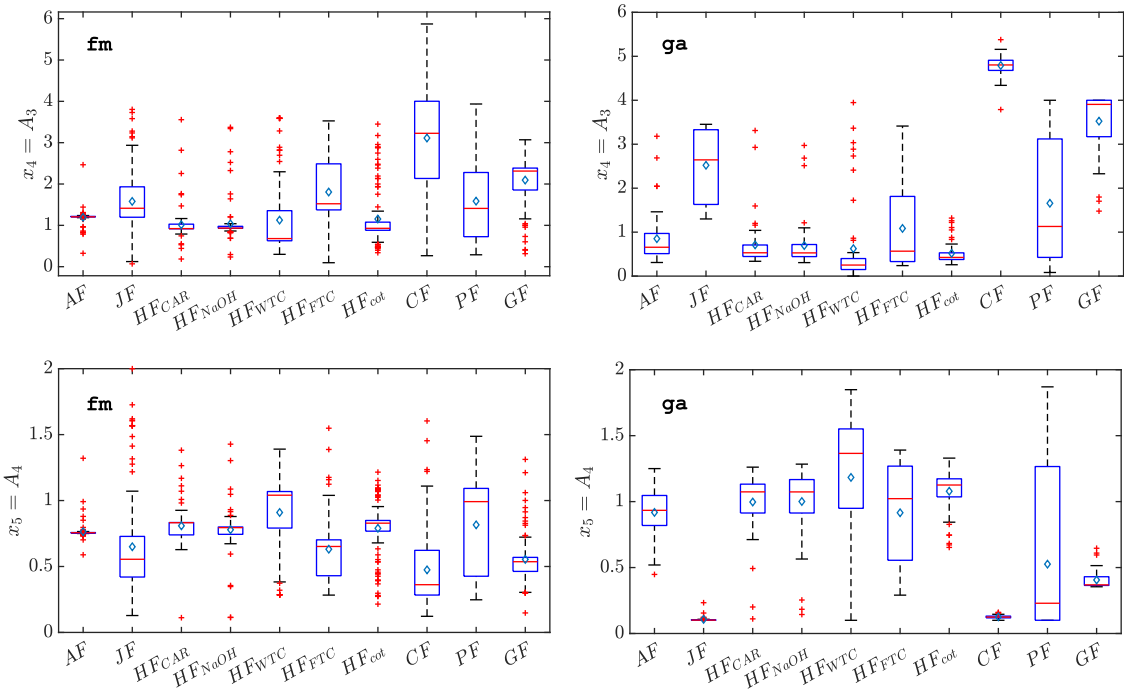

FIG. 8. Statistical distribution associated with the design parameters $x_4 = A_3$ and $x_5 = A_4$ obtained with the `fm` and `ga` solvers.

TABLE III. Design variables obtained from a second iteration of the optimization using two different solvers.

ID	Solver	r_e (μm)	A_1 (−)	A_2 (−)	A_3 (−)	A_4 (−)
AF	fm	33.6 ± 0.0	0.065 ± 0.0	1.372 ± 0.0	1.209 ± 0.0	0.755 ± 0.0
	ga	34.2 ± 0.2	0.074 ± 0.0	1.322 ± 0.0	0.911 ± 0.0	0.838 ± 0.0
JF	fm	26.2 ± 0.0	0.034 ± 0.0	1.798 ± 0.0	1.501 ± 0.0	0.508 ± 0.0
	ga	25.9 ± 0.0	0.057 ± 0.0	1.608 ± 0.0	3.330 ± 0.0	0.101 ± 0.0
HF_{car}	fm	34.9 ± 0.0	0.054 ± 0.0	1.413 ± 0.0	0.970 ± 0.0	0.785 ± 0.0
	ga	33.3 ± 0.2	0.065 ± 0.0	1.360 ± 0.0	0.689 ± 0.0	0.936 ± 0.0
HF_{NaOH}	fm	36.9 ± 0.2	0.063 ± 0.0	1.358 ± 0.0	0.952 ± 0.0	0.770 ± 0.0
	ga	34.1 ± 0.0	0.080 ± 0.0	1.300 ± 0.0	0.704 ± 0.0	0.925 ± 0.0
HF_{WTC}	fm	21.6 ± 0.1	0.090 ± 0.0	1.237 ± 0.0	0.841 ± 0.0	0.947 ± 0.0
	ga	20.6 ± 0.1	0.114 ± 0.0	1.168 ± 0.0	0.358 ± 0.0	1.288 ± 0.0
HF_{FTC}	fm	20.2 ± 0.2	0.050 ± 0.0	1.442 ± 0.0	1.959 ± 0.0	0.583 ± 0.0
	ga	19.5 ± 0.0	0.065 ± 0.0	1.358 ± 0.0	1.019 ± 0.1	0.800 ± 0.1
HF_{cot}	fm	20.8 ± 0.0	0.079 ± 0.0	1.322 ± 0.0	0.966 ± 0.1	0.809 ± 0.1
	ga	20.8 ± 0.0	0.071 ± 0.0	1.363 ± 0.0	0.882 ± 0.1	0.832 ± 0.1
CF	fm	13.8 ± 0.3	0.062 ± 0.0	1.258 ± 0.0	2.277 ± 0.0	0.391 ± 0.0
	ga	13.1 ± 0.0	0.056 ± 0.0	1.363 ± 0.0	4.909 ± 0.1	0.100 ± 0.1
PF	fm	16.1 ± 0.6	0.063 ± 0.0	1.343 ± 0.0	0.820 ± 0.0	0.020 ± 0.0
	ga	15.9 ± 0.0	0.050 ± 0.0	1.508 ± 0.0	3.040 ± 0.0	0.324 ± 0.0
GF	fm	8.6 ± 0.1	0.146 ± 0.0	0.995 ± 0.0	2.210 ± 0.0	0.530 ± 0.0
	ga	8.5 ± 0.0	0.111 ± 0.0	1.087 ± 0.0	4.000 ± 0.0	0.558 ± 0.0

and 20%, except for *JF*, which shows a difference of above 30%. For all the materials, a higher consistency is found for the variable A_2; deviations between the two solvers never exceed 10%. Generally, larger deviations are observed for A_3 and A_4, particularly for fibers *JF*, HF_{WTC}, CF, and PF, where, for at least one of these variables, deviations exceed 50%.

The significant deviations found in some cases for the variables associated with the characteristic lengths, while strong consistency is observed for the effective radius (maximum deviation around 5%), can be attributed to the differing influence of the transport parameters on the JCA model's computation of the sound absorption coefficient. A small deviation in airflow resistivity, dependent on the effective radius, may lead to a noticeable variation in the sound absorption coefficient. In contrast, deviations observed in the characteristic lengths have a small or negligible effect on the sound absorption coefficient spectra, as demonstrated in the results presented in Fig. 5 and the Appendix. Even though these deviations suggest large differences between the estimates from the two solvers, they refer to relatively small values, and the results are within the same order of magnitude.

V. CONCLUSION

This paper presents a novel optimization technique for the fast and reliable characterization of fibrous materials and the optimization of their density. The proposed methodology, which requires only the measurement of the normal incidence sound absorption coefficient, can potentially be implemented in-house or in commercial measurement software. It finds useful application in the design and optimization of sound absorption panels, significantly reducing the need for extensive prototyping phases. The presented method is applicable to any type of fibrous material; however, it is not suitable for porous or granular materials. The method integrates an optimization algorithm with the JCA model, providing a straightforward characterization technique that can be easily implemented in any acoustic laboratory, as it only requires the experimental measurement of the normal incidence sound absorption coefficients of the sample at different compression ratios.

This study comprehensively validates the proposed optimization methodology using Posidonia fibers. The results demonstrate that the methodology provides reliable estimates of key transport parameters, such as airflow resistivity, tortuosity, and characteristic lengths, when compared to established analytical and inversion-based methods. For airflow resistivity, in particular, the validation shows slight deviations of the optimized results from analytical values. These deviations are attributed to inherent assumptions in the model, particularly regarding fiber orientation. Despite these deviations, the proposed approach maintains good consistency and accuracy across a range of porosities.

The comparison between experimental and simulated sound absorption coefficients using the JCA model further confirms the robustness of the methodology. The close alignment between the experimental data and the simulation results across different porosities highlights the reliability of the transport parameters derived from the proposed optimization technique. Moreover, the applicability of the proposed technique to a broad range of fibrous materials, including both traditional and natural fibers, is investigated using nine additional materials. The results, presented in the Appendix, demonstrate the technique's versatility and reliability in estimating the transport parameters of fibrous media and accurately describing their acoustic behavior through the JCA model.

https://doi.org/10.1121/10.0035847

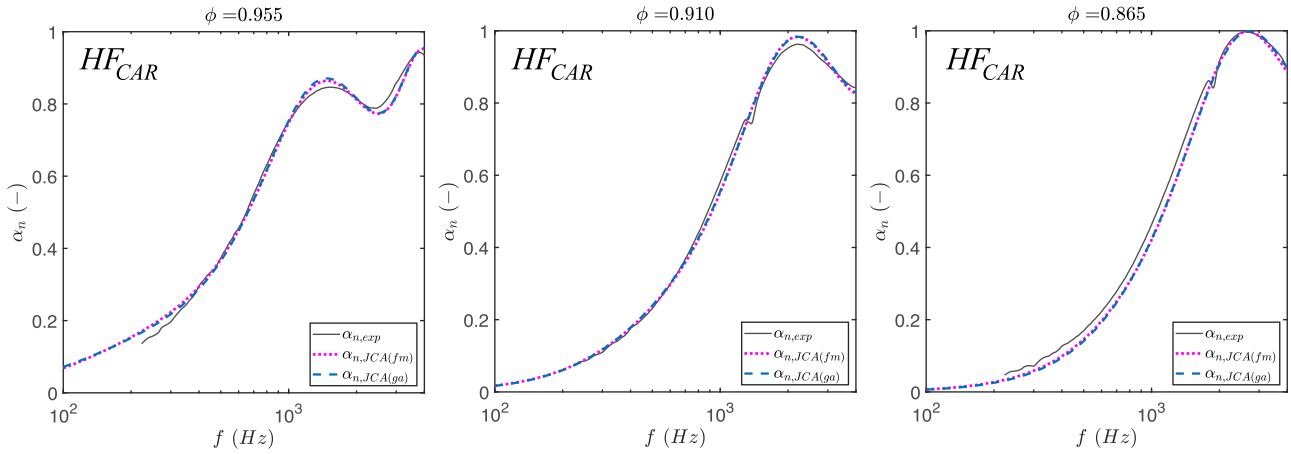

FIG. 10. Fibers HF_{CAR}. Comparison for different values of porosity ϕ between the experimental normal incidence sound absorption coefficient $\alpha_{n,\mathrm{exp}}$ and the JCA model simulations using the inverted transport parameters obtained either from `fm` and `ga` solvers: $\alpha_{nJCA,fm}$, $\alpha_{nJCA,ga}$.

Additionally, the study explores the influence of the search space on optimization outcomes using two different solvers. The findings suggest that the genetic algorithm (ga) generally provides more consistent results compared to the non-linear solver (`fm`), particularly in reducing the risk of convergence to local minima. However, the non-linear solver also demonstrates robustness when proper search space boundaries are applied. Since the algorithm boundaries cannot be known *a priori*, a preliminary parametric multi-run optimization over a broad range of values can be employed to refine the search space. In this study, this was achieved through a statistical analysis, where the refined boundaries were identified using the IQR of results obtained from the preliminary parametric optimization. This approach allows for good consistency in the results obtained with the two solvers, especially in the evaluation of the effective radius, which is used to determine the airflow resistivity. More variability is found in the other design variables, on which the characteristic lengths depend. However, the estimated variables always remain within the same order of magnitude, and the observed differences do not significantly influence the results in terms of the sound absorption coefficient.

Overall, the proposed optimization approach is validated as a reliable and accurate method for estimating transport parameters in porous fibrous materials. This method can be effectively applied across various fibrous materials used in acoustic mitigation systems, ensuring consistency in sound absorption predictions. The results suggest that careful management of the search space and solver selection are critical to achieving optimal and physically meaningful outcomes.

AUTHOR DECLARATIONS

Conflict of Interest

The authors report no conflict of interest.

DATA AVAILABILITY

The data that support the findings of this study are available from the corresponding author upon reasonable request.

APPENDIX: APPLICATION TO OTHER FIBROUS MATERIALS

To evaluate the accuracy of the proposed inversion technique across a broad range of fibrous materials, we

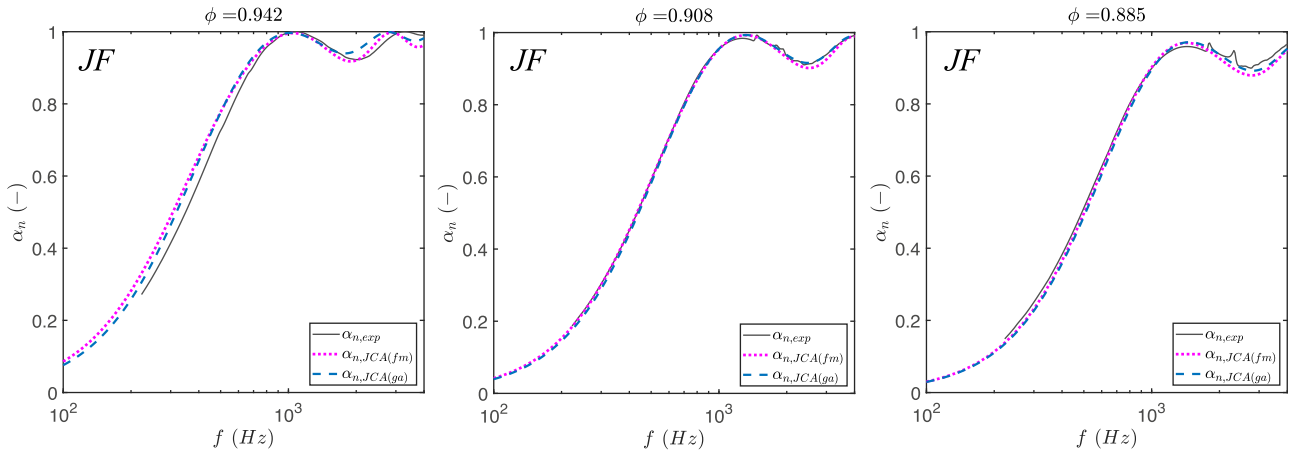

FIG. 9. Fibers JF. Comparison for different values of porosity ϕ between the experimental normal incidence sound absorption coefficient $\alpha_{n,\mathrm{exp}}$ and the JCA model simulations using the inverted transport parameters obtained either from `fm` and `ga` solvers: $\alpha_{nJCA,fm}$, $\alpha_{nJCA,ga}$.

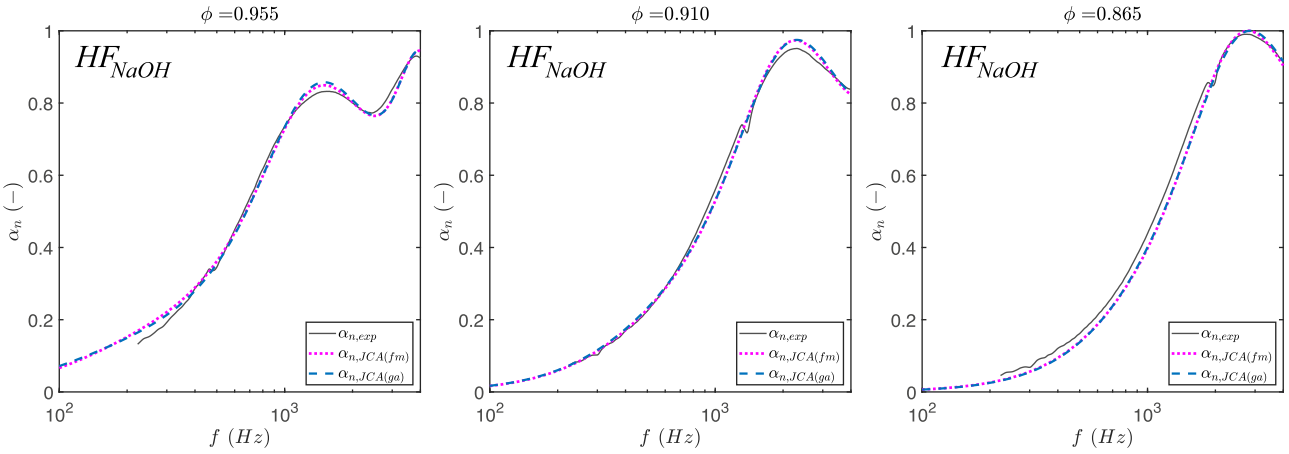

FIG. 11. Fibers HF_{NaOH}. Comparison for different values of porosity ϕ between the experimental normal incidence sound absorption coefficient $\alpha_{n,\mathrm{exp}}$ and the JCA model simulations using the inverted transport parameters obtained either from `fm` and `ga` solvers: $\alpha_{n,JCA,fm}$, $\alpha_{n,JCA,ga}$.

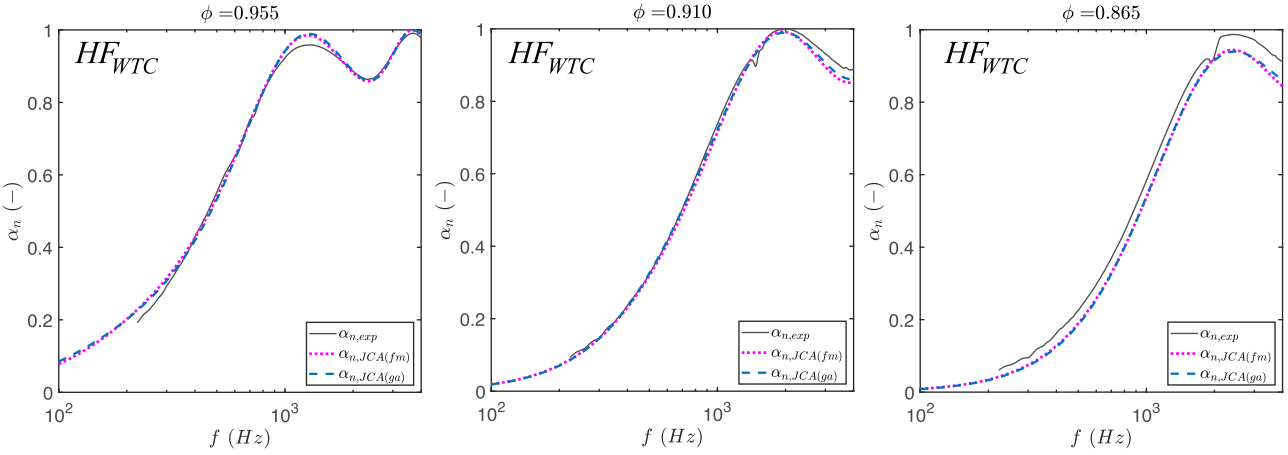

FIG. 12. Fibers HF_{WTC}. Comparison for different values of porosity ϕ between the experimental normal incidence sound absorption coefficient $\alpha_{n,\mathrm{exp}}$ and the JCA model simulations using the inverted transport parameters obtained either from `fm` and `ga` solvers: $\alpha_{n,JCA,fm}$, $\alpha_{n,JCA,ga}$.

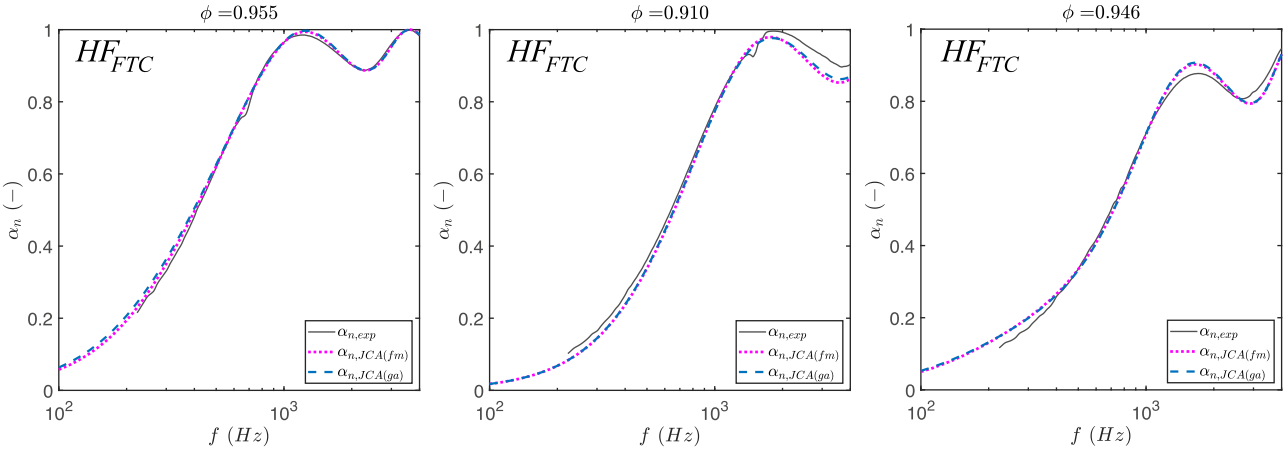

FIG. 13. Fibers HF_{FTC}. Comparison for different values of porosity ϕ between the experimental normal incidence sound absorption coefficient $\alpha_{n,\mathrm{exp}}$ and the JCA model simulations using the inverted transport parameters obtained either from `fm` and `ga` solvers: $\alpha_{n,JCA,fm}$, $\alpha_{n,JCA,ga}$.

https://doi.org/10.1121/10.0035847

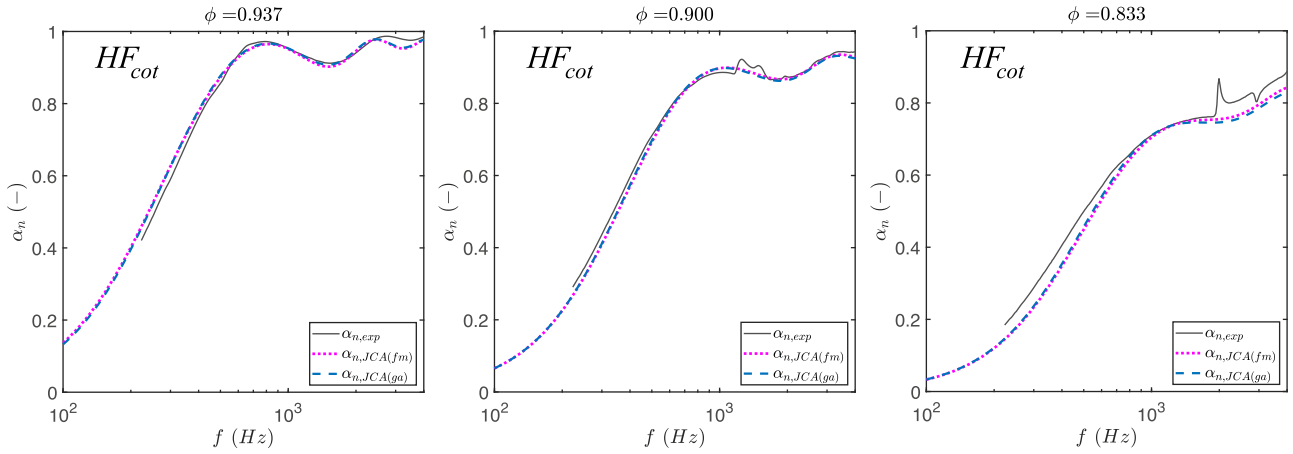

FIG. 14. Fibers HF_{cot}. Comparison for different values of porosity ϕ between the experimental normal incidence sound absorption coefficient $\alpha_{n,\exp}$ and the JCA model simulations using the inverted transport parameters obtained either from `fm` and `ga` solvers: $\alpha_{nJCA,fm}$, $\alpha_{nJCA,ga}$.

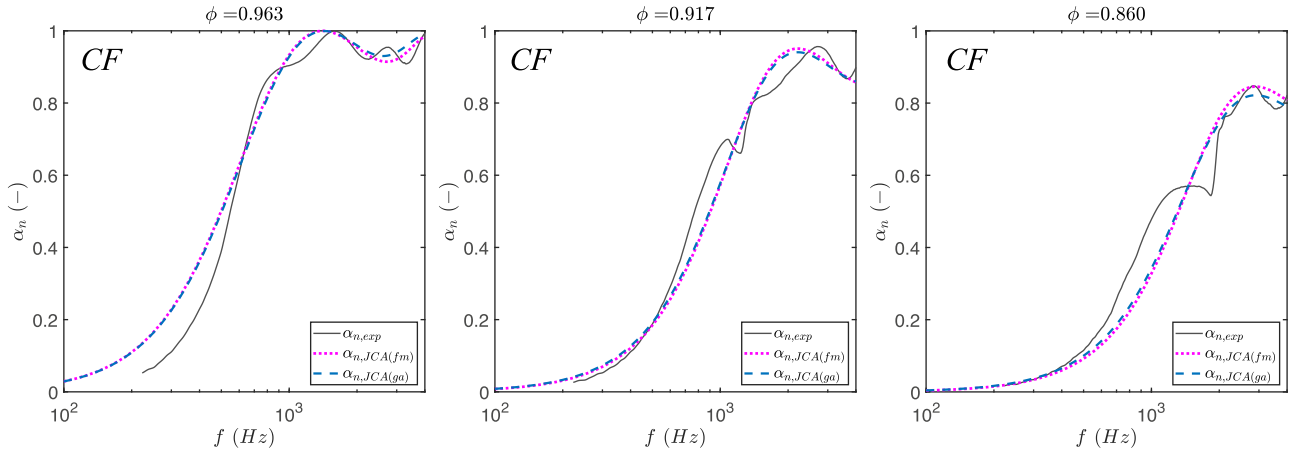

FIG. 15. Fibers CF. Comparison for different values of porosity ϕ between the experimental normal incidence sound absorption coefficient $\alpha_{n,\exp}$ and the JCA model simulations using the inverted transport parameters obtained either from `fm` and `ga` solvers: $\alpha_{nJCA,fm}$, $\alpha_{nJCA,ga}$.

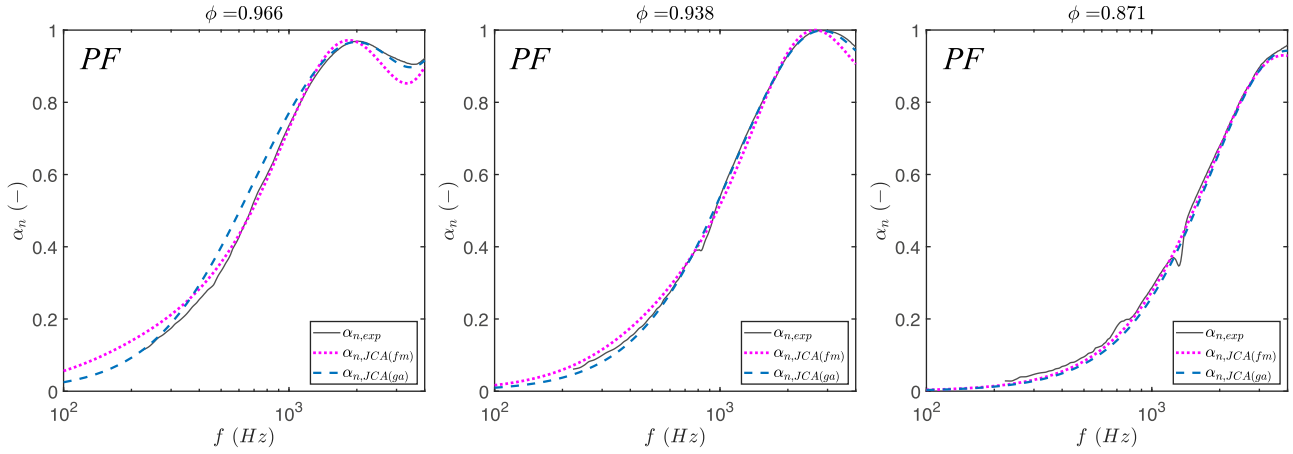

FIG. 16. Fibers PF. Comparison for different values of porosity ϕ between the experimental normal incidence sound absorption coefficient $\alpha_{n,\exp}$ and the JCA model simulations using the inverted transport parameters obtained either from `fm` and `ga` solvers: $\alpha_{nJCA,fm}$, $\alpha_{nJCA,ga}$.

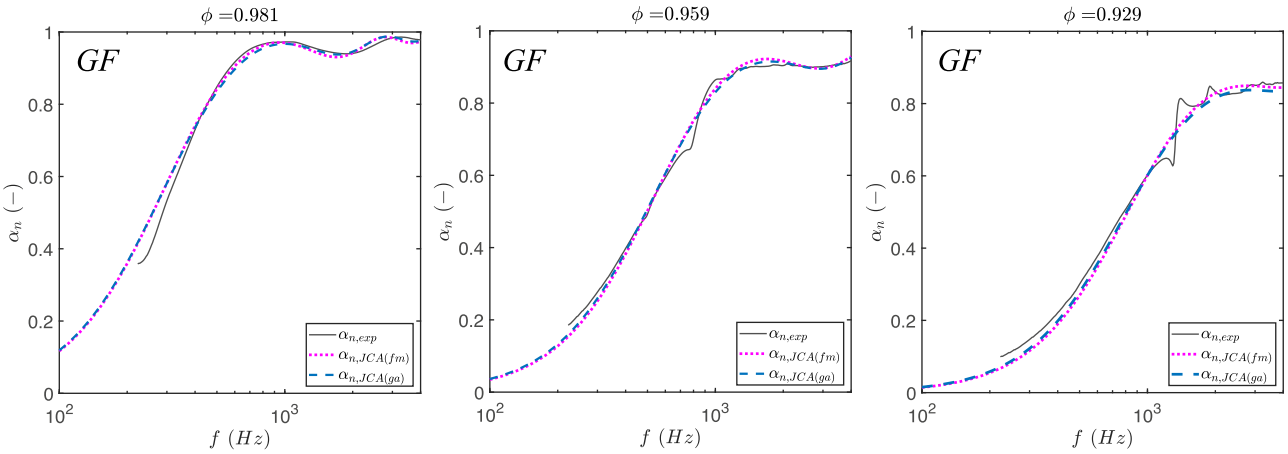

FIG. 17. Fibers GF. Comparison for different values of porosity ϕ between the experimental normal incidence sound absorption coefficient $\alpha_{n,\mathrm{exp}}$ and the JCA model simulations using the inverted transport parameters obtained either from `fm` and `ga` solvers: $\alpha_{n,JCA,fm}$, $\alpha_{n,JCA,ga}$.

applied the method to ten additional fibers commonly used in acoustic mitigation systems. The accuracy of the methodology was further assessed by comparing the experimental normal incidence sound absorption coefficients with the simulated results from the JCA model for these additional materials, as listed in Table II. The results are presented for various porosity values in Figs. 9–17. The transport parameters computed using Eqs. (8)–(11), based on the design variables provided in Table III, allow for accurate predictions of the normal incidence sound absorption coefficients across all the investigated materials, including both natural-based and traditional fibers. Consistent with the observations from Fig. 5, larger deviations between the predicted and experimental results are systematically noted at the lowest and highest porosity values. Small differences are observed between the results obtained using the `fm` and `ga` solvers within the optimization algorithm, with the sound absorption coefficient spectra associated with both solvers generally overlapping. The larger differences observed at high frequencies for materials CF and PF (Figs. 15 and 16) are linked to deviations in the coefficients A_3 and A_4 obtained from the two solvers, from which the thermal characteristic length is computed. In these cases, the ga solver provides a slightly better approximation of the experimental results. Nonetheless, the discrepancies are minimal, and both solvers yield results that closely match the experimental sound absorption coefficients. Even in cases where the sound absorption spectra are characterized by peaks and dips due to sample resonances, the model provides a good approximation of the experimental data. This indicates that the proposed methodological approach reliably estimates the transport parameters, ensuring accurate predictions of the sound absorption coefficients through the JCA model.

[1]R. Panneton and E. Gros, "A missing mass method to measure the open porosity of porous solids," Acta Acust. Acust. **91**(2), 342–348 (2005), available at https://www.scopus.com/record/display.uri?eid=2-s2.0-17044385042&origin=recordpage.
[2]Y. Salissou and R. Panneton, "Pressure/mass method to measure open porosity of porous solids," J. Appl. Phys. **101**(12), 124913 (2007).
[3]J. F. Allard, B. Castagnede, M. Henry, and W. Lauriks, "Evaluation of tortuosity in acoustic porous materials saturated by air," Rev. Sci. Instrum. **65**(3), 754–755 (1994).
[4]Z. E. A. Fellah, S. Berger, W. Lauriks, C. Depollier, C. Aristegui, and J.-Y. Chapelon, "Measuring the porosity and the tortuosity of porous materials via reflected waves at oblique incidence," J. Acoust. Soc. Am. **113**(5), 2424–2433 (2003).
[5]P. Leclaire, L. Kelders, W. Lauriks, C. Glorieux, and J. Thoen, "Determination of the viscous characteristic length in air-filled porous materials by ultrasonic attenuation measurements," J. Acoust. Soc. Am. **99**(4), 1944–1948 (1996).
[6]K. V. Horoshenkov, "A review of acoustical methods for porous material characterisation," Int. J. Acoust. Vib. **22**(1), 92–103 (2017).
[7]E. Di Giulio, C. Perrot, and R. Dragonetti, "Transport parameters for sound propagation in air saturated motionless porous materials: A review," Int. J. Heat Fluid Flow **108**, 109426 (2024).
[8]K. V. Horoshenkov, A. Khan, F.-X. Bécot, L. Jaouen, F. Sgard, A. Renault, N. Amirouche, F. Pompoli, N. Prodi, P. Bonfiglio, G. Pispola, F. Asdrubali, J. Hübelt, N. Atalla, C. K. Amédin, W. Lauriks, and L. Boeckx, "Reproducibility experiments on measuring acoustical properties of rigid-frame porous media (round-robin tests)," J. Acoust. Soc. Am. **122**(1), 345–353 (2007).
[9]F. Pompoli, P. Bonfiglio, K. V. Horoshenkov, A. Khan, L. Jaouen, F.-X. Bécot, F. Sgard, F. Asdrubali, F. D'Alessandro, J. Hübelt, N. Atalla, C. K. Amédin, W. Lauriks, and L. Boeckx, "How reproducible is the acoustical characterization of porous media?," J. Acoust. Soc. Am. **141**(2), 945–955 (2017).
[10]ISO 9053-1:2018, "Acoustics: Determination of airflow resistance. 1. Static airflow method" (International Organization for Standardization, Geneva, Switzerland, 2018).
[11]ISO 9053-2:2020, "Acoustics: Determination of airflow resistance. 1. Alternating airflow method" (International Organization for Standardization, Geneva, Switzerland, 2018).
[12]R. Panneton and X. Olny, "Acoustical determination of the parameters governing viscous dissipation in porous media," J. Acoust. Soc. Am. **119**(4), 2027–2040 (2006).
[13]X. Olny and R. Panneton, "Acoustical determination of the parameters governing thermal dissipation in porous media," J. Acoust. Soc. Am. **123**(2), 814–824 (2008).
[14]P. Bonfiglio and F. Pompoli, "Inversion problems for determining physical parameters of porous materials: Overview and comparison between different methods," Acta Acust. Acust. **99**(3), 341–351 (2013).
[15]L. Jaouen, E. Gourdon, and P. Glé, "Estimation of all six parameters of Johnson-Champouxallard-Lafarge model for acoustical porous materials from impedance tube measurements," J. Acoust. Soc. Am. **148**(4), 1998–2005 (2020).
[16]D. L. Johnson, J. Koplik, and R. Dashen, "Theory of dynamic permeability and tortuosity in fluid-saturated porous media," J. Fluid Mech. **176**, 379–402 (1987).

https://doi.org/10.1121/10.0035847

[17]Y. Champoux and J.-F. Allard, "Dynamic tortuosity and bulk modulus in air-saturated porous media," J. Appl. Phys. **70**(4), 1975–1979 (1991).
[18]M. E. Delany and E. Bazley, "Acoustical properties of fibrous absorbent materials," Appl. Acoust. **3**(2), 105–116 (1970).
[19]Y. Miki, "Acoustical properties of porous materials-modifications of Delany-Bazley models," J. Acoust. Soc. Jpn. (E) **11**(1), 19–24 (1990).
[20]ISO 10534-2:2023, "Acoustics: Determination of acoustic properties in impedance tubes: 2. Two-microphone technique for normal sound absorption coefficient and normal surface impedance" (International Organization for Standardization, Geneva, Switzerland, 2023).
[21]D. Lafarge, P. Lemarinier, J. F. Allard, and V. Tarnow, "Dynamic compressibility of air in porous structures at audible frequencies," J. Acoust. Soc. Am. **102**(4), 1995–2006 (1997).
[22]C. Zwikker and C. W. Kosten, *Sound Absorbing Materials*, 2nd ed. (Elsevier, Amsterdam, 1949).
[23]J. Allard and N. Atalla, *Propagation of Sound in Porous Media: Modelling Sound Absorbing Materials*, 2nd ed. (Wiley, Chichester, UK, 2009).
[24]A. Tamayol and M. Bahrami, "Transverse permeability of fibrous porous media," Phys. Rev. E **83**(4), 046314 (2011).
[25]F. Pompoli and P. Bonfiglio, "Definition of analytical models of non-acoustical parameters for randomly-assembled symmetric and asymmetric radii distribution in parallel fiber structures," Appl. Acoust. **159**, 107091 (2020).
[26]A. Santoni, P. Bonfiglio, P. Fausti, C. Marescotti, V. Mazzanti, F. Mollica, and F. Pompoli, "Improving the sound absorption performance of sustainable thermal insulation materials: Natural hemp fibres," Appl. Acoust. **150**, 279–289 (2019).
[27]H. T. Luu, R. Panneton, and C. Perrot, "Effective fiber diameter for modeling the acoustic properties of polydisperse fiber networks," J. Acoust. Soc. Am. **141**(2), EL96–EL101 (2017).
[28]Q. V. Tran, C. Perrot, R. Panneton, M. T. Hoang, L. Dejaeger, V. Marcel, and M. Jouve, "Effect of polydispersity on the transport and sound absorbing properties of threedimensional random fibrous structures," Int. J. Solids Struct. **296**, 112840 (2024).
[29]B. Castagnede, A. Aknine, B. Brouard, and V. Tarnow, "Effects of compression on the sound absorption of fibrous materials," Appl. Acoust. **61**(2), 173–182 (2000).
[30]K. Hirosawa and H. Nakagawa, "Formulae for predicting non-acoustical parameters of deformed fibrous porous materials," J. Acoust. Soc. Am. **141**(6), 4301–4313 (2017).
[31]L. Lei, N. Dauchez, and J. Chazot, "Prediction of the six parameters of an equivalent fluid model for thermocompressed glass wools and melamine foam," Appl. Acoust. **139**, 44–56 (2018).
[32]G. E. Archie, "The electrical resistivity log as an aid in determining some reservoir characteristics," Trans. AIME **146**(1), 54–62 (1942).
[33]H. T. Luu, C. Perrot, and R. Panneton, "Influence of porosity, fiber radius and fiber orientation on the transport and acoustic properties of random fiber structures," Acta Acust. Acust. **103**(6), 1050–1063 (2017).
[34]F. Pompoli, "Acoustical characterization and modeling of sustainable Posidonia fibers," Appl. Sci. **13**(7), 4562 (2023).
[35]N. Karmarkar, "A new polynomial-time algorithm for linear programming," in *Proceedings of the Sixteenth Annual ACM Symposium on Theory of Computing* (1984), pp. 302–311.
[36]A. Antoniou and W.-S. Lu, *Practical Optimization: Algorithms and Engineering Applications*, 2nd ed. (Springer, New York, 2021).
[37]J. H. Holland, *Adaptation in Natural and Artificial Systems: An Introductory Analysis with Applications to Biology, Control, and Artificial Intelligence* (Massachusetts Institute of Technology, Cambridge, MA, 1992).
[38]A. Messac, *Optimization in Practice with MATLAB: For Engineering Students and Professionals* (Cambridge University Press, London, 2015).
[39]A. Santoni, P. Bonfiglio, A. Magnani, C. Marescotti, F. Pompoli, and P. Fausti, "A hybrid approach for modelling the acoustic properties of recycled fibre mixtures for automotive applications," Appl. Acoust. **182**, 108272 (2021).
[40]O. Doutres, Y. Salissou, N. Atalla, and R. Panneton, "Evaluation of the acoustic and non-acoustic properties of sound absorbing materials using a three-microphone impedance tube," Appl. Acoust. **71**(6), 506–509 (2010).